Supplementary Information for "Constant-Overhead Fault-Tolerant Bell-Pair Distillation using High-Rate Codes"

J. Pablo Bonilla Ataides,[1,*] Hengyun Zhou,[2] Qian Xu,[3,4]
Gefen Baranes,[1,5] Bikun Li,[6] Mikhail D. Lukin,[1,†] and Liang Jiang[6,‡]

[1] *Department of Physics, Harvard University, Cambridge, MA 02138, USA*
[2] *QuEra Computing Inc., Boston, MA 02135, USA*
[3] *Institute for Quantum Information and Matter, Caltech, Pasadena, CA, USA*
[4] *Walter Burke Institute for Theoretical Physics, Caltech, Pasadena, CA, USA*
[5] *Department of Physics and Research Laboratory of Electronics, Massachusetts Institute of Technology, Cambridge, MA, USA*
[6] *Pritzker School of Molecular Engineering, The University of Chicago, Chicago, Illinois 60637, USA*

CONTENTS

1. RELATED WORK

We expand on several relevant Bell-pair distillation methods using the criteria introduced in the main text.

- **BDSW-1EPP** [1]: A one-way "hashing" method capable of achieving a constant rate equal to the Hashing bound of the channel. The rate is given by $R = 1 - H(p)$, where the Von-Neumann entropy of the error channel is:

$$H(p) = -(1-p)\log_2(1-p) - p\log_2\left(\frac{p}{3}\right).$$

  At a Bell-Pair infidelity of 5% (1%), the rate is 0.63 (0.90). The protocol relies on random quantum codes, for which no efficient decoding methods are currently known, rendering it impractical with existing tools.

- **BDSW-2EPP** [1]: A two-way distillation method with a vanishing asymptotic rate. The protocol can be considered as a subset of Ref. [2], where the concatenated code is the [2,1,2] classical repetition code in alternating X and Z bases. The scheme is not robust against gate errors, as it un-encodes to physical Bell pairs.

- **Ramette et al.** [3]: A lattice-surgery-based one-way distillation scheme. Since the scheme is based on surface codes it has a vanishing rate. At an input Bell infidelity of 5% (1%), the rate is lower than 1/5300 (1/1300) to achieve a target logical error rate of 10^{-12} [2]. A total of $O(d^2)$ Bell pairs must be shared at the boundary for surface codes of distance d. The lattice surgery protocol requires a circuit of depth d, where each step consumes d Bell pairs. The boundary threshold, where the Bell pairs reside, is approximately 10%, while the bulk threshold, where local qubits reside, is approximately 1%. Other lattice surgery proposals [4–6] share similar performance metrics.

- **Shi et al.** [7]: A fault-tolerant encoder with a non-fault-tolerant un-encoder for qLDPC codes. This scheme requires two-way communication: Alice sends data to Bob for encoding, and Bob sends data back to Alice for decoding. The method does not require additional qubits beyond those of the qLDPC code (and potentially some local ancillas). However, it does not consider specific high-rate qLDPC codes, and no threshold simulations are performed.

- **Pattison et al.** [2]: A two-way error-detecting method that achieves a constant rate through concatenation of small codes. Due to concatenation and post-selection, this method may require a large buffer memory, as faulty Bell pairs are discarded. The resulting encoding memory overhead scales as $O\left((\log\log 1/\epsilon)^{\alpha \log\log 1/\epsilon}\right) > O(1)$, for an output error rate ϵ and some $\alpha > 0$. At an input Bell infidelity of 5% (1%), and assuming a buffer memory of 50 logical qubits, the protocol achieves a rate of 16.53 (7.32) to reach a target logical error rate of 10^{-12}.

- **Gu et al.** [8] (concurrent with our work): A two-way error-detecting method that achieves a constant rate using random bilocal Clifford circuits. The scheme requires a buffer memory of $\log_2(1/\epsilon)^{3/2}$ qubits for each Alice and Bob, for an output error rate ϵ. Assuming noiseless local operations, it can achieve an overhead of 7 at an input Bell-pair infidelity of 10%, reaching a target logical error rate of 10^{-12}. The scheme can be made robust to local gate errors by injecting Bell pairs into a QEC code at each node.

- **This work**: A deterministic (one-way) constant-rate distillation protocol based on high-rate qLDPC codes. The resource overhead is constant, as the scheme requires no additional Bell pairs beyond those used in the qLDPC block, along with $O(1)$ local ancillas. The output Bell pairs remain encoded in the qLDPC code, making the scheme robust against local gate noise. Since the same qLDPC code is used for both distillation and local gate noise suppression, the entire fault-tolerant pipeline can be simulated. We analyze various schemes:

  – A family of HGP codes with a rate $\geq 4\%$ and a threshold of 10%, below which the Bell-pair error can be arbitrarily suppressed.

  – A family of LP codes with a rate $\sim 11\%$, with four finite-size instances constructed, and a threshold of $\sim 10\%$.

  – A rate $\sim 1/3$ code with a pseudothreshold of 7.5%, achieving a logical error rate of $\sim 10^{-12}$ at an input Bell error rate of 1% (extrapolated from the subthreshold fitted ansatz).

  See the End Matter of the main text for full results.

We note that while various other purification methods exist [9–22], a detailed comparison of these methods is left for future work.

2. NOISE MANIPULATION

In this section, we analyze how Bell-pair depolarizing noise and circuit noise transform under different setups, leading to effective noise models for our numerical simulations.

2.1. Depolarizing noise

Consider a Bell pair with one qubit at Alice's node and the other at Bob's node:

$$|\Phi^+\rangle = \frac{1}{\sqrt{2}}(|0\rangle_A \otimes |0\rangle_B + |1\rangle_A \otimes |1\rangle_B)$$

Each qubit undergoes a depolarizing channel with error probability p_{bell}:

$$\mathcal{E}_p^{\text{A}}(\rho_{\text{AB}}) = (1 - p_{\text{bell}})\rho_{\text{AB}} + \frac{p_{\text{bell}}}{3} \sum_{P \in \{X,Y,Z\}} P_{\text{A}} \rho_{\text{AB}} P_{\text{A}},$$

$$\mathcal{E}_p^{\text{B}}(\rho_{\text{AB}}) = (1 - p_{\text{bell}})\rho_{\text{AB}} + \frac{p_{\text{bell}}}{3} \sum_{P \in \{X,Y,Z\}} P_{\text{B}} \rho_{\text{AB}} P_{\text{B}}.$$

We seek an equivalent noise model where Alice's side is noiseless, and Bob's side has an effective depolarizing error p'_{bell} (Fig. S1). In Table I, we enumerate all possible Pauli operator configurations resulting from the depolarizing channels on Alice's and Bob's sides and the corresponding resulting Bell states. By summing the probabilities of these configurations, we determine the likelihood of each Bell state for both the original (left) and modified (right) setups. Equating the probabilities of each Bell state in the two setups provides a consistent solution for the effective error parameter: $p'_{\text{bell}} = 2p_{\text{bell}} - \frac{4}{3}p_{\text{bell}}^2$.

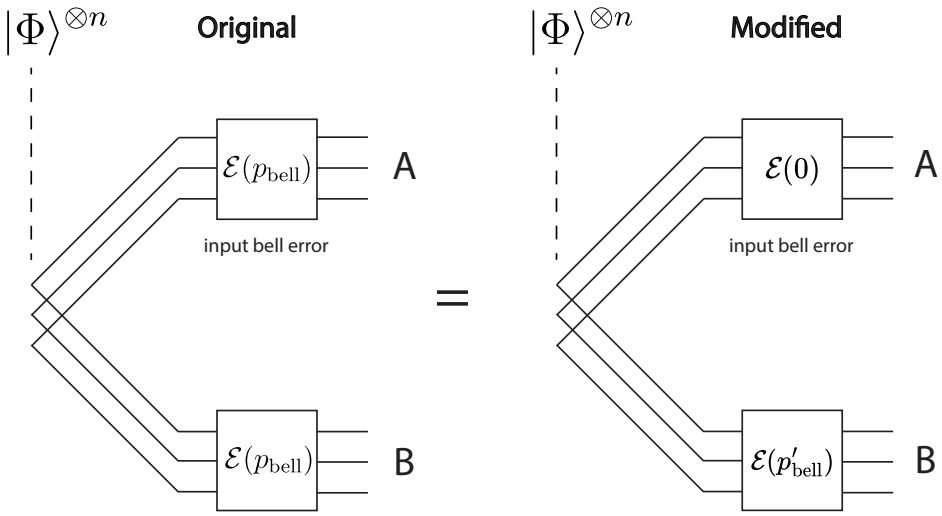

FIG. S1. Bell error equivalence. The left setup represents the original configuration where both Alice and Bob experience input Bell pair depolarizing noise $\mathcal{E}(p_{\text{bell}})$. The right setup illustrates the equivalent modified configuration where Alice's side is noiseless $\mathcal{E}(0)$, and Bob's side has an effective increased depolarizing error $\mathcal{E}(p'_{\text{bell}})$.

2.2. Circuit noise

Suppose we run the same circuit on each leg of the Bell pair. The error channel is parametrized by an error strength p, such that physical operations in the circuit fail with probability p, or some constant factor of p. Consider the two

Bell state	Error Mechanisms (original)	Probability (original)	Error Mechanisms (modified)	Probability (modified)
$\|\Phi^+\rangle$	$I_\mathrm{A}I_\mathrm{B}, X_\mathrm{A}X_\mathrm{B}, Y_\mathrm{A}Y_\mathrm{B}, Z_\mathrm{A}Z_\mathrm{B}$	$(1-p_\mathrm{bell})^2 + \frac{p_\mathrm{bell}^2}{3}$	I_B	$1-p'_\mathrm{bell}$
$\|\Phi^-\rangle$	$I_\mathrm{A}Z_\mathrm{B}, Z_\mathrm{A}I_\mathrm{B}, X_\mathrm{A}Y_\mathrm{B}, Y_\mathrm{A}X_\mathrm{B}$	$\frac{2p_\mathrm{bell}}{3}(1-p_\mathrm{bell}) + \frac{2p_\mathrm{bell}^2}{9}$	Z_B	$\frac{p'_\mathrm{bell}}{3}$
$\|\Psi^+\rangle$	$I_\mathrm{A}X_\mathrm{B}, X_\mathrm{A}I_\mathrm{B}, Y_\mathrm{A}Z_\mathrm{B}, Z_\mathrm{A}Y_\mathrm{B}$	$\frac{2p_\mathrm{bell}}{3}(1-p_\mathrm{bell}) + \frac{2p_\mathrm{bell}^2}{9}$	X_B	$\frac{p'_\mathrm{bell}}{3}$
$\|\Psi^-\rangle$	$I_\mathrm{A}Y_\mathrm{B}, Y_\mathrm{A}I_\mathrm{B}, X_\mathrm{A}Z_\mathrm{B}, Z_\mathrm{A}X_\mathrm{B}$	$\frac{2p_\mathrm{bell}}{3}(1-p_\mathrm{bell}) + \frac{2p_\mathrm{bell}^2}{9}$	Y_B	$\frac{p'_\mathrm{bell}}{3}$

TABLE I. Pauli operators and the resulting Bell states. Summary of the Pauli operators acting on Alice's and Bob's sides, their corresponding Bell states, and the probabilities of each configuration under the depolarizing noise model for the original and modified setups. The probabilities of the Bell states in the original and modified setups are equated to derive the effective error parameter $p'_\mathrm{bell} = 2p_\mathrm{bell} - \frac{4}{3}p_\mathrm{bell}^2$.

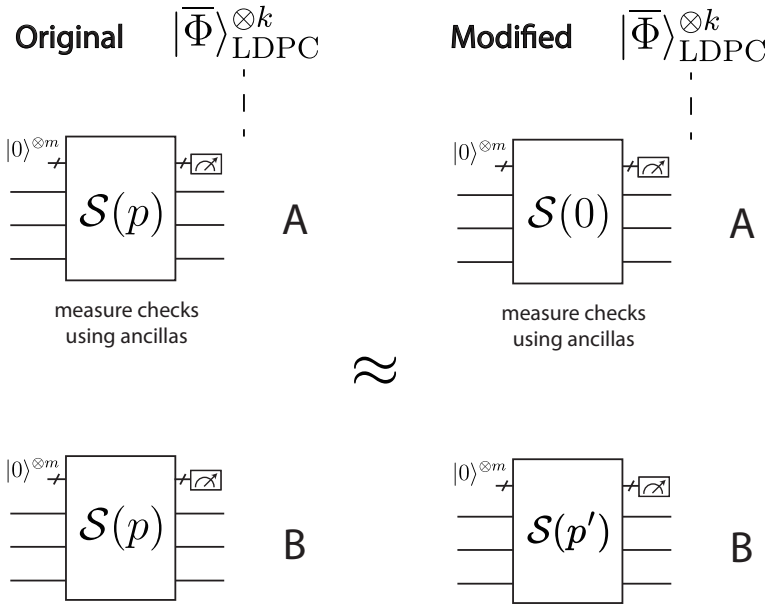

FIG. S2. Circuit error approximation. The left setup shows the original configuration, where both Alice and Bob's circuits experience errors characterized by $\mathcal{S}$. The right setup illustrates the modified configuration, where Alice's circuit is noiseless $\mathcal{S}(0)$, and Bob's circuit has an effective increased error strength $\mathcal{S}(p')$.

setups shown in Fig. S2. On the left, the error channels on Alice's and Bob's sides are identical, each with the error parameter p. On the right, Alice's circuit is noiseless, and Bob's circuit has an effective error parameter p'. Our goal is to relate p' to p, using reasoning similar to the previous section.

The circuits are error correction circuits, where syndrome extraction is performed using bare, local ancilla qubits, as described in the main text. The logical operators and resulting logical Bell states are consistent with those presented in Table I.

For this analysis, we focus on logical operators that result in a $|\bar{\Phi}^-\rangle$ state, though the results apply to any row in Table I. Specifically, we seek to relate p' and p under the condition that a logical $\bar{Z}$ error occurs. In the modified setup, the probability of a logical error, $\mathbb{P}_p(\bar{Z})$, at sufficiently low physical error rates is given by summing over all possible error configurations. This can be expressed as a sum over circuit fault weights ω, with an entropy factor, A_ω accounting for the number of weight-ω error configurations that lead to a logical failure:

$$\mathbb{P}_{p'}(\bar{Z}) \approx \sum_\omega A_\omega (p')^\omega.$$

In the original setup, each weight-ω error configuration that leads to failure in the modified setup also leads to failure. However, there is an additional degeneracy: each physical error can occur on either Alice's or Bob's side, yet the logical effect remains the same due to the joint decoding of Alice's and Bob's syndromes. For example, consider a 4-qubit repetition code, where $ZZII$ results in a logical $\bar{Z}$ error. In the joint code (with stabilizers $s \otimes s$, where s is

a stabilizer in the original code, as derived in the main text), the modified setup allows only the configuration:

$$(IIII) \otimes (ZZII).$$

In contrast, the original setup exhibits a 2^2-fold degeneracy as the following configurations all lead to a logical $\bar{Z}$ error (ignoring higher weight corrections [23]):

$$(IIII) \otimes (ZZII) \quad (ZZII) \otimes (IIII) \quad (ZIII) \otimes (IZII) \quad (IZII) \otimes (ZIII).$$

More generally, for any weight-ω error configuration in the modified setup, there are 2^ω equivalent weight-ω configurations in the original setup. Thus, the probability of a logical $\bar{Z}$ error in the original setup, ignoring higher weight corrections, is:

$$\mathbb{P}_p(\bar{Z}) \approx \sum_\omega A_\omega 2^\omega p^\omega.$$

By equating the probabilities $\mathbb{P}_{p'}(\bar{Z}) = \mathbb{P}_p(\bar{Z})$ we obtain:

$$p' \approx 2p.$$

At very low physical error rates, where weight-$\sim d/2$ error configurations dominate, our approximations becomes increasingly tight.

2.3. Generalizations

2.3.1. Combination of Bell and Circuit Errors

To incorporate both Bell depolarizing errors and circuit gate errors into a unified framework, we analyze the entire protocol within the circuit error model. In this framework, the Bell depolarizing error acts as a preparation error on the input qubits, which can equivalently be represented as perfect initialization followed by a Pauli error. Thus, the results from the previous sections apply simultaneously to both Bell depolarizing and gate errors, justifying the use of $p' \approx 2p$ and $p'_{\text{bell}} \approx 2p_{\text{bell}}$.

2.3.2. Generalization to Multiple Cycles

In the limit of a large number of QEC cycles on both sides, the system effectively behaves as two independent logical qubits. For such independent logical qubits, the logical error rate per round scales as:

$$f(p') = 2 \times f(p),$$

whereas our approximation assumes

$$f(p') = f(2p),$$

which provides a conservative upper bound on the actual error rate. This holds because:

$$f(p) = (p/p_{\text{th}})^{d/2}$$

is a high power function. Therefore, $p' \approx 2p$ provides a reasonable conservative estimate for the case of multiple QEC cycles.

3. CODE CONSTRUCTIONS

3.1. Hypergraph product code

HGP codes are a class of quantum low-density parity-check (qLDPC) codes derived from the Cartesian product of two classical LDPC codes [24]. Let the parity-check matrices of the classical codes be $H_1 \in \mathbb{F}_2^{r_1 \times n_1}$ and $H_2 \in \mathbb{F}_2^{r_2 \times n_2}$, where r_1, r_2 are the number of checks, and n_1, n_2 are the number of bits. The quantum stabilizer matrices are given by:

$$H_X = \begin{bmatrix} H_1^T \otimes I_{r_2} & I_{n_1} \otimes H_2 \end{bmatrix}, \quad H_Z = \begin{bmatrix} I_{r_1} \otimes H_2^T & H_1 \otimes I_{n_2} \end{bmatrix},$$

where $\otimes$ denotes the Kronecker product. This construction guarantees the CSS condition $H_X H_Z^T = 0$.

For classical codes with parameters $[n_i, k_i, d_i]$, where $r_i = n_i - k_i$ are the linearly-independent checks, the resulting HGP code encodes $k = k_1 k_2$ logical qubits into $n = n_1 n_2 + r_1 r_2$ physical qubits, with distance $d = \min(d_1, d_2)$. If the classical codes are repetition codes $[n, 1, O(n)]$, the HGP construction yields the surface code. If, instead, the classical codes encode a constant number of logical bits $[n, O(n), O(n)]$, the HGP construction yields constant-rate codes with square-root distance $[[n, O(n), O(\sqrt{n})]]$.

In this work, the classical codes are constructed using (3,4)-regular Tanner graphs [25–27], which are bipartite graphs where each bit node has degree 3 and each check node has degree 4. We generate candidate (3,4)-regular Tanner graphs via rejection sampling, selecting the best one based on:

- **High girth** (≥ 6) to minimize short cycles, improving decoder performance.
- **Large spectral gap**, which enhances expansion properties and is associated with single-shot QEC.
- **Maximum code distance**, ensuring improved error correction performance.

By varying the size of the Tanner graph, we construct a family of classical codes $C_1, C_2, \ldots$, from which we derive a family of quantum codes by taking the hypergraph product of the classical code with itself, $Q = \text{HGP}(C, C)$:

$$Q_1 = [[225, 9, 4]], \quad Q_2 = [[625, 25, 6]], \quad Q_3 = [[1225, 49, 8]], \quad \ldots$$

These codes achieve a minimum rate of $k/n \geq 4\%$. The HGP codes used in this article are the same as those studied in Ref. [25].

The structure of HGP codes lends itself to a compact implementation protocol using reconfigurable atom arrays [25]. Since lifted-product (LP) and spatially-coupled (SC) codes are built using HGP codes, the optimized movement schemes developed for HGP codes can also aid the implementation of the LP and SC codes.

3.2. Lifted product code

Quasi-cyclic lifted Product (LP) codes are a family of quantum low-density parity-check (qLDPC) codes that enhance the hypergraph product by introducing a lifting operation [28–30]. This operation uses cyclic group structures to reduce the number of required qubits while maintaining high code rates and robust error-correcting properties.

LP codes are constructed using two classical base protographs, represented by matrices B_1 and B_2 over the quotient polynomial ring $R[x]/(x^l - 1)$. These matrices generate larger matrices B_x and B_z:

$$B_x = \begin{bmatrix} B_1^T \otimes I_{m_{B2}} & I_{n_{B1}} \otimes B_2 \end{bmatrix}, \quad B_z = \begin{bmatrix} I_{m_{B1}} \otimes B_2^T & B_1 \otimes I_{n_{B2}} \end{bmatrix}.$$

Here, l denotes the lift size, and B_1, B_2 correspond to the underlying protographs of size $m_{B1} \times n_{B1}$ and $m_{B2} \times n_{B2}$, respectively. The "lifting" operation replaces each element of B_x and B_z with its corresponding circulant $l \times l$ matrix representation. This process generates the H_X and H_Z stabilizer matrices required for the quantum code, ensuring that $H_X H_Z^T = 0$.

The LP code has parameters $[[n, k, d]]$, where:

- $n = l(n_{B1} n_{B2} + m_{B1} m_{B2})$,

- $k = l(n_{B1}n_{B2} + m_{B1}m_{B2} - m_{B1}n_{B2} - n_{B1}m_{B2})$, and
- d is the minimum distance, upper bounded by the classical distance of the lifted base matrix.

We construct LP codes using base matrices B_1 and B_2 with monomial entries and size 3×5. To optimize the LP codes, the base matrices are selected to maximize girth (≥ 8) and distance. To form a code family, we vary the lift size $l = 16, 21, 30, 42$, obtaining base matrices B_1, B_2, B_3, B_4 with classical distances $d = 12, 16, 20, 24$:

$$\mathbf{B}_1 = \begin{bmatrix} 1 & 1 & 1 & 1 & 1 \\ 1 & x^2 & x^4 & x^7 & x^{11} \\ 1 & x^3 & x^{10} & x^{14} & x^{15} \end{bmatrix}, \quad \mathbf{B}_2 = \begin{bmatrix} 1 & 1 & 1 & 1 & 1 \\ 1 & x^4 & x^5 & x^7 & x^{17} \\ 1 & x^{14} & x^{18} & x^{12} & x^{11} \end{bmatrix}, \quad \mathbf{B}_3 = \begin{bmatrix} 1 & 1 & 1 & 1 & 1 \\ 1 & x^2 & x^{14} & x^{24} & x^{25} \\ 1 & x^{16} & x^{11} & x^{14} & x^{13} \end{bmatrix}, \quad \mathbf{B}_4 = \begin{bmatrix} 1 & 1 & 1 & 1 & 1 \\ 1 & x^6 & x^7 & x^9 & x^{30} \\ 1 & x^{40} & x^{15} & x^{31} & x^{35} \end{bmatrix}$$

and associated quantum code parameters $[[544, 80, \leq 12]]$, $[[714, 100, \leq 16]]$, $[[1020, 136, \leq 20]]$, $[[1428, 184, \leq 24]]$.

The constructed LP codes achieve encoding rates lower-bounded by 2/17 and distances matching the underlying classical matrices with high probability. This LP code construction follows the same method used in Ref. [30] and Ref. [25].

3.3. Spatially-coupled code

Spatially Coupled Quantum Low-Density Parity-Check (SC-qLDPC) codes extend classical spatially coupled (SC) codes to the quantum setting [31, 32]. Following Ref. [32], we outline the construction of the SC codes used in this work.

At a high level, SC codes can be viewed as LP codes with an additional coupling structure, where the lifted matrices are stacked vertically and horizontally in a repeating pattern. This procedure reduces excess physical qubits while maintaining a large number of encoded logical qubits, thereby increasing the code rate. A partitioning matrix $\mathbf{P}$ is used to decompose the base matrix $\mathbf{B}$ into $m+1$ component matrices, each of which is lifted according to a lifting matrix $\mathbf{L}$, generating the lifted component matrices H_i $(i = 0, 1, \ldots, m)$. These component matrices are then stacked vertically to form a so-called replica, and the replicas are stacked horizontally to form the full check matrix H. For a class of SC codes known as tail-biting (TB) codes, the resultant check matrix is given by:

$$\mathbf{H} = \begin{bmatrix} H_0 & 0 & \cdots & 0 & H_m & \cdots & H_1 \\ H_1 & H_0 & 0 & \cdots & 0 & \ddots & \vdots \\ \vdots & H_1 & H_0 & \ddots & \vdots & \ddots & H_m \\ H_m & \vdots & \ddots & 0 & 0 & \cdots & 0 \\ 0 & H_m & \ddots & H_1 & H_0 & \ddots & \vdots \\ \vdots & \ddots & \ddots & \vdots & H_1 & \ddots & 0 \\ 0 & \cdots & 0 & H_m & \cdots & H_1 & H_0 \end{bmatrix}$$

Here, m is known as the memory of the SC code, and the coupling length L refers to the number of columns of H.

A Two-Dimensional (2D) SC code extends the 1D SC structure by coupling multiple SC codes together. A memory-m_1 SC code is constructed from $m_1 + 1$ component matrices, each of which is itself a memory-m_2 SC code. The final code is characterized by outer and inner coupling lengths, L_1 and L_2, respectively. The check matrix is then specified by check matrices H_{ij}, where $i = 0, 1, \ldots, m_1$ and $j = 0, 1, \ldots, m_2$.

The Toric code is an example of a 2D-SC code, where $(m_1, m_2, L_1, L_2) = (1, 1, d, d)$. For instance, the $d = 3$ Toric code has parity-check matrix:

$$\mathbf{H}_{\text{Toric}} = \left[\begin{array}{ccc|ccc|ccc} A & & B & & & & C & & D \\ B & A & & & & & D & C & \\ & B & A & & & & & D & C \\ \hline C & & D & A & & B & & & \\ D & C & & B & A & & & & \\ & D & C & & B & A & & & \\ \hline & & & C & & D & A & & B \\ & & & D & C & & B & A & \\ & & & & D & C & & B & A \end{array}\right],$$

where the block matrices are:

$$\mathbf{A} = \begin{bmatrix} X & I \\ I & I \end{bmatrix}, \quad \mathbf{B} = \begin{bmatrix} X & X \\ Z & I \end{bmatrix}, \quad \mathbf{C} = \begin{bmatrix} I & X \\ Z & Z \end{bmatrix}, \quad \text{and} \quad \mathbf{D} = \begin{bmatrix} I & I \\ I & Z \end{bmatrix}.$$

3.3.1. Algebraic formulation

The algebraic formulation for SC codes facilitates the construction of the code we use. At its core is the characteristic function, $F(U,V)$, which determines the component matrices H_{ij} of the final parity-check matrix:

$$F(U,V) = \sum_{i=0}^{m_1} \sum_{j=0}^{m_2} H_{ij} U^i V^j.$$

For 2D SC-HGP codes, the characteristic function takes a form similar to the hypergraph product:

$$\mathbf{F}(U,V) = \begin{bmatrix} X\big(I_{n_2\times n_2} \otimes \mathbf{A}(U,V)\big) & X\big(\bar{\mathbf{B}}(U,V)^T \otimes I_{r_1\times r_1}\big) \\ Z\big(\mathbf{B}(U,V) \otimes I_{n_1\times n_1}\big) & Z\big(I_{r_2\times r_2} \otimes \bar{\mathbf{A}}(U,V)^T\big) \end{bmatrix},$$

where $\mathbf{A}(U,V) \in \mathbb{F}_2^{r_1\times n_1}[U,V]$ and $\mathbf{B}(U,V) \in \mathbb{F}_2^{r_2\times n_2}[U,V]$. One may interpret $\mathbf{F}(U,V)$ as the hypergraph product of $\mathbf{A}$ and $\mathbf{B}$. For each of $\mathbf{A}$ and $\mathbf{B}$, there exists an associated partitioning matrix $\mathbf{P}_a$ and $\mathbf{P}_b$ that fully determine the final partitioning matrix $\mathbf{P}$, which itself is the hypergraph product of $\mathbf{P}_a$ and $\mathbf{P}_b$.

To construct the final SC-HGP code, we begin with base matrices $\mathbf{A}$ and $\mathbf{B}$ of size $r_1 \times n_1$ and $r_2 \times n_2$, respectively, memories m_1 and m_2 and coupling lengths L_1 and L_2. Applying the hypergraph product, the resulting check matrix has $r = r_1 n_2 + r_2 n_1$ rows and $n = r_1 r_2 + n_1 n_2$ columns, encoding at least $k = n - r = (n_1 - r_1)(n_2 - r_2)$ logical qubits. After spatial coupling, the final matrix has $N = (r_1 r_2 + n_1 n_2) L_1 L_2$ physical qubits and encodes at least $K = (n_1 - r_1)(n_2 - r_2) L_1 L_2$ logical qubits.

For the SC-HGP code construction used in this paper, the following parameters are used:

$$r_1 = r_2 = 3, \quad n_1 = n_2 = 7, \quad m_1 = m_2 = 3, \quad L_1 = L_2 = 10.$$

The partitioning matrices, analogous to base classical codes in HGP codes, are optimized to remove cycles using the Gradient Descent (GRADE) - Algorithmic Optimization (AO) method. After GRADE-AO optimization, the resulting code eliminates cycles-4 and cycles-6 entirely and reduces the number of cycles-8 to 380.

The resulting 2D-SC-HGP code encodes 1624 logical qubits into 5800 physical qubits, yielding a rate of 0.28. The value 1624 exceeds the minimum $K = 1600$ predicted earlier due to the presence of linearly dependent checks.

Ref. [32] also constructs a $[[7300, 2500]]$ SC-HGP code. However, due to the difficulty in simulating the smaller $[[5800, 1624]]$ code at the circuit level, we did not explore simulating the larger one. We leave this to future work, along with developing a full family of SC codes.

4. NUMERICAL SIMULATIONS

To estimate the threshold error rate, we use the critical exponent ansatz [33], which approximates the logical error rate as:

$$\bar{P} = A + Bx + Cx^2,$$

where $x = (p - p_{\text{th}}) d^{\alpha}$, p_{th} is the threshold error rate, d is the code distance, and α is a critical exponent.

For the results shown in the main text, the fitted parameters for the HGP code family are:

$$\begin{aligned} A &= 0.058 \pm 0.002, \qquad B = 0.10 \pm 0.02, \qquad C = 0.05 \pm 0.02, \\ p_{\text{th}} &= 0.108 \pm 0.001, \qquad \alpha = 1.6 \pm 0.1. \end{aligned}$$

For the LP code family, the fitted parameters are:

$$A = 0.037 \pm 0.001, \qquad B = 0.32 \pm 0.03, \qquad C = 0.7 \pm 0.2,$$
$$p_{\text{th}} = 0.103 \pm 0.001, \qquad \alpha = 0.67 \pm 0.04.$$

* jbonillaataides@g.harvard.edu
† lukin@physics.harvard.edu
‡ liangjiang@uchicago.edu

[1] C. H. Bennett, D. P. DiVincenzo, J. A. Smolin, and W. K. Wootters, Physical Review A **54**, 3824 (1996).
[2] C. A. Pattison, G. Baranes, J. Ataides, M. D. Lukin, and H. Zhou, arXiv preprint arXiv:2408.15936 (2024).
[3] J. Ramette, J. Sinclair, N. P. Breuckmann, and V. Vuletic, arXiv preprint arXiv:2302.01296 (2023).
[4] A. G. Fowler, D. S. Wang, C. D. Hill, T. D. Ladd, R. V. Meter, and L. C. L. Hollenberg, Physical Review Letters **104**, 180503 (2010).
[5] J. Sinclair, J. Ramette, B. Grinkemeyer, D. Bluvstein, M. Lukin, and V. Vuletić, arXiv preprint arXiv:2408.08955 (2024).
[6] H. Leone, S. Srikara, P. P. Rohde, and S. Devitt, arXiv preprint arXiv:2209.00151 (2024), arXiv:2209.00151 [quant-ph].
[7] Y. Shi, A. Patil, and S. Guha, arXiv preprint arXiv:2408.06299 (2024).
[8] A. Gu, L. Leone, K. Goodenough, and S. Khatri, arXiv preprint arXiv:2502.09483 (2025), arXiv:2502.09483 [quant-ph].
[9] C. H. Bennett, G. Brassard, S. Popescu, B. Schumacher, J. A. Smolin, and W. K. Wootters, Physical Review Letters **76**, 722 (1996).
[10] M. Murao, M. B. Plenio, S. Popescu, V. Vedral, and P. L. Knight, Physical Review A **57**, R4075 (1998).
[11] K. Vollbrecht and F. Verstraete, Physical Review A **71**, 10.1103/PhysRevA.71.062325 (2005).
[12] N. Isailovic, Y. Patel, M. Whitney, and J. Kubiatowicz, arXiv preprint arXiv:quant-ph/0604048 (2006), arXiv:quant-ph/0604048 [quant-ph].
[13] E. Hostens, J. Dehaene, and B. De Moor, Physical Review A **73**, 10.1103/PhysRevA.73.062337 (2006).
[14] A. W. Leung and P. W. Shor, arXiv preprint arXiv:quant-ph/0702155 (2007), arXiv:quant-ph/0702155 [quant-ph].
[15] P. Hayden, M. Horodecki, A. Winter, and J. Yard, Open Systems & Information Dynamics **15**, 7 (2008).
[16] A. W. Leung, Phys. Rev. A **77**, 012322 (2008).
[17] S. Krastanov, V. V. Albert, and L. Jiang, Quantum **3**, 123 (2019).
[18] C. Gidney, arXiv preprint arXiv:2311.10971 (2023), arXiv:2311.10971 [quant-ph].
[19] K. Goodenough, A. Sajjad, E. Kaur, S. Guha, and D. Towsley, arXiv preprint arXiv:2406.02427 (2024), arXiv:2406.02427 [quant-ph].
[20] N. Rengaswamy, N. Raveendran, A. Raina, and B. Vasić, Quantum **8**, 1233 (2024).
[21] V. Siddhu, D. Abdelhadi, T. Jochym-O'Connor, and J. Smolin, arXiv preprint arXiv:2405.06231 (2024), arXiv:2405.06231 [quant-ph].
[22] Y. Shi, A. Patil, and S. Guha, Measurement-based entanglement distillation and constant-rate quantum repeaters over arbitrary distances (2025), arXiv:2502.11174 [quant-ph].
[23] We note that there are higher weight terms that can also lead to failure - for example, $(XZII) \otimes (YIII)$. We ignore these higher weight corrections when deriving our approximation for p'.
[24] J. P. Tillich and G. Zemor, IEEE Transactions on Information Theory **60**, 1193 (2014).
[25] Q. Xu, J. P. Bonilla Ataides, C. A. Pattison, N. Raveendran, D. Bluvstein, J. Wurtz, B. Vasić, M. D. Lukin, L. Jiang, and H. Zhou, Nature Physics , 1 (2024).
[26] M. A. Tremblay, N. Delfosse, and M. E. Beverland, Physical Review Letters **129**, 050504 (2022).
[27] A. Grospellier, L. Grouès, A. Krishna, and A. Leverrier, Quantum **5**, 432 (2021).
[28] P. Panteleev and G. Kalachev, Quantum **5**, 585 (2019).
[29] N. P. Breuckmann and J. N. Eberhardt, IEEE Transactions on Information Theory **67**, 6653 (2020).
[30] N. Raveendran, N. Rengaswamy, F. Rozpędek, A. Raina, L. Jiang, and B. Vasić, Quantum **6**, 767 (2022).
[31] M. Hagiwara, K. Kasai, H. Imai, and K. Sakaniwa, in *2011 IEEE International Symposium on Information Theory Proceedings*, IEEE (IEEE, 2011) pp. 638–642.
[32] S. Yang and R. Calderbank, arXiv preprint arXiv:2305.00137 (2023).
[33] C. Wang, J. Harrington, and J. Preskill, Annals of Physics **303**, 31 (2003).